

## Article

# Improvements in the Characterisation of Permeability and Inertial Factor of Insect-Proof Screens through Pressure Drop Coefficients

Francisco-Javier Granados-Ortiz <sup>1,2,\*</sup>, Alejandro López-Martínez <sup>2,3</sup> , Francisco Domingo Molina-Aiz <sup>2,3</sup> , Choi-Hong Lai <sup>4</sup>, Araceli Peña-Fernández <sup>2,3</sup> , Juan Antonio Martínez-Lao <sup>2,5</sup> and Diego Luis Valera-Martínez <sup>2,3</sup> 

<sup>1</sup> Department of Mechanical, Thermal and Fluid Engineering, University of Málaga C/ Dr Ortiz Ramos s/n, 29071 Málaga, Spain

<sup>2</sup> Department of Engineering, University of Almería, 04120 La Cañada, Spain

<sup>3</sup> CIAIMBITAL Research Centre, University of Almería, 04120 La Cañada, Spain

<sup>4</sup> School of Computing and Mathematical Sciences, University of Greenwich, London SE10 9LS, UK

<sup>5</sup> CIMEDES Research Center (CeIA3), University of Almería, 04120 La Cañada, Spain

\* Correspondence: fgranados@ual.es

**Abstract:** Permeability and inertial factor are the most relevant variables in the Forchheimer equation. They are important to estimate pressure drop when a fluid flow is passing through a porous media. However, in the insect-proof screens field, the existing models to date are still providing a poor predictive accuracy, in part due to they are based on 2D porosity of screens. This work provides novel models for permeability and inertial factor, which are developed from experimental data of insect-proof screens in a wind tunnel and the analytical estimation of 3D porosity. Instead of fitting models directly on observed training data values of permeability and inertial factor, we propose to focus the modelling efforts on finding models dependent on the 3D porosity through the constants in the pressure drop of Forchheimer equation. Since two screens can have the same 2D porosity but different 3D porosity, this makes also models more reliable. The combination of all these aspects has led to parametric models that overcome by far predictions by previous models in the literature.

**Keywords:** insect-proof screens; permeability; aerodynamic characterisation; inertial factor; porous medium



**Citation:** Granados-Ortiz, F.-J.; López-Martínez, A.; Molina-Aiz, F.D.; Lai, C.-H.; Peña-Fernández, A.; Martínez-Lao, J.A.; Valera-Martínez, D.L. Improvements in the Characterisation of Permeability and Inertial Factor of Insect-Proof Screens through Pressure Drop Coefficients. *Agronomy* **2023**, *13*, 602. <https://doi.org/10.3390/agronomy13020602>

Academic Editor: Andrea Sciarretta

Received: 15 December 2022

Revised: 8 February 2023

Accepted: 14 February 2023

Published: 20 February 2023



**Copyright:** © 2023 by the authors. Licensee MDPI, Basel, Switzerland. This article is an open access article distributed under the terms and conditions of the Creative Commons Attribution (CC BY) license (<https://creativecommons.org/licenses/by/4.0/>).

## 1. Introduction

Insect-proof screens (IPS) are a physical barrier used as protection from insects in ventilation openings such as buildings and greenhouses. This element is typically built as interlaced threads forming a fabric-like screen, with warp and weft threads [1]. The use of these screens is extensive in greenhouses on the Mediterranean coast. For instance, they are used in greenhouses at the southeast of the Spanish peninsula [2], where IPSs are placed in ventilation openings. Thanks to the installation of IPSs, harmful insects are prevented from entering [3,4] and beneficial insects are prevented from leaving [3]. The main drawback of its use is the reduction of natural ventilation capacity in greenhouses [5–7], due to the significant pressure drop caused by their presence [1] also leads to a drastic reduction in airflow energy passing through the IPS [8]. e.g., In a greenhouse with IPSs it was identified more temperature and humidity levels [6], and lower airflow velocity [9], than in a greenhouse without IPSs. The scenario described for greenhouses is actually quite similar in standard homes with IPSs installed in windows (although with different temperature and humidity levels). Thus, other important applications of these screens are homes to get a passive protection of humans from insects [10], or even in farms with the purpose of protecting animals from diseases transmitted by insects and bugs [11]. Another important consequence of using insect-proof screens is mixing enhancement [8]. However, mixing is not as strong as in other more intense mixing applications [12,13].

Once the importance of IPSs has been identified, there is a real need to characterise them geometrically and aerodynamically, due to their impact in ventilation. The design of the IPSs pursues two counterpart objectives: (i) to define an adequate pore geometry to prevent the passage of small insects; (ii) to ensure that such pore geometry has the least possible effect on ventilation capacity. It is essential to accurately study the geometry of the pores, their effect on the passage of particles/objects/insects and their effect on the flow that passes through them, in order to use this information to optimise the design of these elements according to the performance that is required.

The first step to characterise the aerodynamics of IPSs is to get information of their geometry. In [14,15] a methodology was published to obtain the 2D geometric parameters of screens. From digital images of IPSs, the thread density, diameter of the threads in both directions ( $D_{hx}$  and  $D_{hy}$ ), length of the pores in both directions or separation between x and y-threads ( $L_{px}$  and  $L_{py}$ ), surface of the pores ( $S_p$ ), the diameter of the circumference inscribed in the pore ( $D_i$ ), and the two-dimensional porosity ( $\phi_{2D}$ ) is obtained. Despite the strong interest on these parameters to classify screens, this two-dimensional characterization is insufficient, since IPSs are three-dimensional structures. For this reason, we recently released an innovative software [16,17] that allows, from the two-dimensional parameters mentioned above plus the measurement of the thickness of the IPS ( $e$ ), to reconstruct the geometry of the IPS in three-dimensions. The software is also able to accurately calculate the 3D volumetric porosity ( $\phi_{3D}$ ) [17], a parameter never considered before, due to the complexity in its analytical modelling. An example is shown in Figure 1.

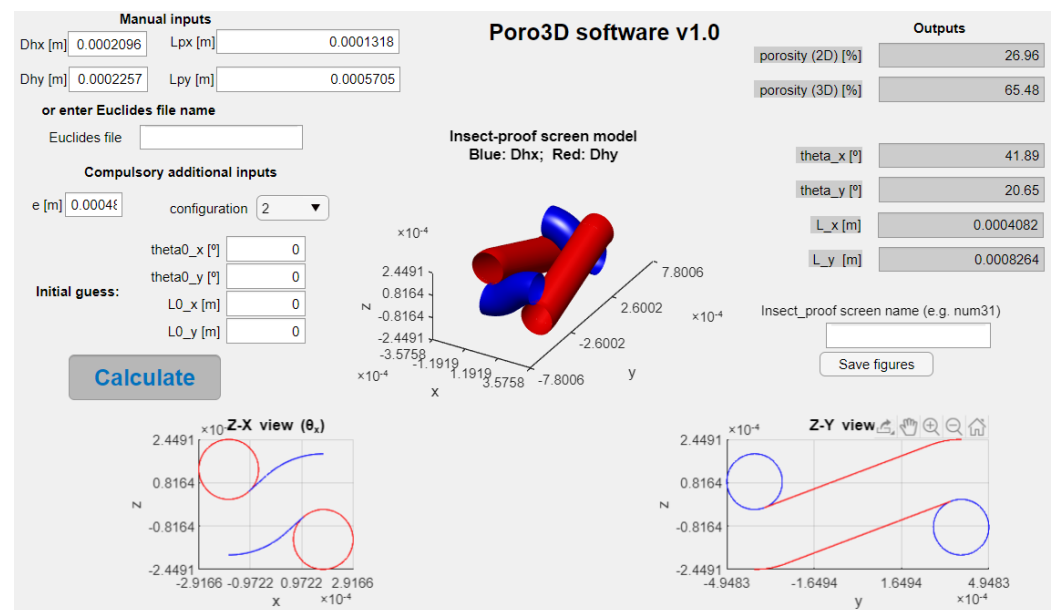


Figure 1. Example of IPS using Pore3D software v1.0 [16].

The second step to characterise the aerodynamics of IPSs is to use the geometric data plus experimental data to build up models to predict the performance of screens. Wind tunnel tests have been carried out to determine the pressure drop caused by the IPSs as a function of airflow velocity [1,18–21]. Pressure drop caused by an IPS can be expressed as a second degree polynomial [1,22]:

$$\Delta P = au^2 + bu, \quad (1)$$

where  $a$  and  $b$  are coefficients which depend on two parameters: (i) permeability,  $K_p$ , which is a function of the geometry of screens; and (ii) inertial factor,  $Y$ , which is a function of the nature of the porous medium [23].

As  $K_p$  and  $Y$  are widely used in aerodynamics, to know more about their impact on ventilation is a must. For this reason, there are many works in the literature which

are focused on the development of models characterise the IPS aerodynamics on this basis [1,3,18,24–26]. In these works, amongst all the important parameters to build their models, porosity of the screens has been found the most influential one. This is so because it has a strong relation to permeability  $K_p$ , and thus, on the inertial factor  $Y$  present in the Forchheimer equation (which is derived from the Darcy equation). This equation can be then further modelled by including  $K_p$  and  $Y$  to fit a second degree polynomial as [1]:

$$\Delta P = \frac{\rho e Y}{\sqrt{K_p}} u^2 + \frac{e \mu}{K_p} u \approx au^2 + bu, \quad (2)$$

where  $\rho$  and  $\mu$  stand for the density and viscosity of air, respectively,  $e$  is the thickness of the screen, and  $u$  is the airflow velocity.

Thus, to determine the value of  $K_p$  and  $Y$  of an IPS experimentally, a wind tunnel is required. Another option is to use models that permit to estimate these aerodynamic parameters based on geometric characteristics only. One of the first attempts to obtain models for  $K_p$  and  $Y$  was the investigation by Miguel [18], who obtained the expressions:  $K_p = 3.44 \times 10^{-9} \phi^{1.6}$ ; and  $Y = 4.3 \times 10^{-2} \phi^{2.13}$ . In a recent work [1], we showed that these equations do not fit well to the IPS performance, and one of the main reasons is that Miguel [18] used data from different types of screens (8 IPS with rectangular pores and circular section wires; and 6 shade screens with irregular pores and flat fibers), thus not being appropriate to obtain generalised models. In a porous medium, the permeability  $K_p$  can be expressed as a function that depends on the porosity and the diameter of the fibres/yarns, by using the Kozeny equation [23]:

$$K_p = \frac{D_h^2 \phi_{2D}^3}{\beta(1 - \phi_{2D})^2}, \quad (3)$$

where  $\beta$  is a constant that depends on the porous medium. From this equation, Lopez et al. [1] obtained a novel expression to estimate  $K_p$  as a function of the two-dimensional porosity and thread diameters:

$$K_p = \frac{D_h^2 \phi_{2D}^3}{2.0679(1 - \phi_{2D})^2} + 3.8362 \times 10^{-10}. \quad (4)$$

The inertial factor  $Y$  can be expressed as a function that depends on the diameter of the fibres of a porous medium and the size of the pore [23,27]. For an IPS, the proposed expression [23,27] can be used by adapting the diameter of the threads and the diameter of the inner circumference of the pores [1]:

$$Y = A + B \frac{D_h}{D_i}, \quad (5)$$

where  $A$  and  $B$  are two constants that depend on the porous medium. From this equation, Lopez et al. [1] developed the following expression:

$$Y = 0.0051195 + 0.135966 \frac{D_h}{D_i}. \quad (6)$$

Both  $K_p$  and  $Y$  aforementioned expressions by Lopez et al. [1] allow to predict values much closer to the measured data (from wind tunnel tests) compared to the predicted values from Miguel [18] equations. These models, as all models developed in the literature, are obtained by fitting directly  $K_p$  and  $Y$  data. However, despite the improvements in Lopez et al. [1], large errors are still taking place. The present investigation aims at solving this research gap, by proposing novel models for  $K_p$  and  $Y$  based on three-dimensional porosity of the screens (generalisable to any IPSs) by modelling through the coefficients of the Forchheimer equation (Equation (2)) with three-dimensional porosity, which provide a much higher level of accuracy and demonstrates that the classical two-dimensional

modelling approach is insufficient. No studies have been found in the literature in which permeability and inertial factor models have been developed to estimate the aerodynamic properties of IPSs based on 3D volumetric porosity through pressure drop coefficients. The present work is highly innovative in the characterisation of IPSs, as their aerodynamic performance can be predicted with high accuracy by means of the models proposed for permeability and inertial factor (and thus, pressure drop) in this manuscript. The models are fully parametric and interpretable. Instead of fitting models directly on observed values of permeability and inertial factor, as done by all previous authors in the literature (e.g., [1,3,18,24–26]), an innovative approach has been tested by finding models for the constants derived from the pressure drop in Forchheimer equation, and by including the three-dimensional porosity of screens. This has demonstrated to be an important contribution as the predictive accuracy of aerodynamic models is highly enhanced.

All works in the literature (specially agroengineering applications outlined in the literature review) model porosity as a 2D property, by calculating porosity as the ratio between the projected pore surface area,  $S_p$ , and the surface area,  $S_t$ :

$$\phi_{2D} = \frac{L_{px}L_{py}}{(L_{px} + D_{hy})(L_{py} + D_{hx})}, \quad (7)$$

However, as remarked in this introduction, porosity is actually a 3D (volumetric) property. An accurate estimation of volumetric porosity can be achieved by calculating the volume ratio of the pore through the complex geometry:

$$\phi_{3D} = \frac{V_p}{V_t}, \quad (8)$$

where  $V_p$  is the volume of the pore, and  $V_t$  is the total volume. Therefore, the present investigation is of high relevance in the prediction of the performance of screens without even requiring to test them experimentally, which is also an important contribution to design *a la carte* IPSs, according to a desired performance and exclusion of insects/objects of a specific size. The impact of this in terms of applications is quite large, from ventilation of greenhouses or homes, to protective mesh for gas turbine compressors [28] or control of turbulence intensity [29].

This manuscript is structured as follows. In Section 2, the mathematical approach to estimate the three-dimensional shape of the screen and the estimation of volumetric porosity is introduced. In Section 3 the models are developed and applied to estimate the behaviour of real-life insect-proof screens, showing the outstanding performance with respect to previous literature to estimate permeability and inertial factor. A discussion section can be found in Section 4. Finally, in Section 5, the conclusions from this work are given.

## 2. Insect-Proof Screen Model and Estimation of 3D Porosity

The model for inextensible, incompressible and round cross-section interlaced threads was first introduced by Peirce [30]. This model assumes no deformation, which is a good approximation since the threads in typical daily applications are made of hard plastic (usually High-Density Polyethylene in greenhouses applications [31]). The model developed by Peirce is adapted to measurements of IPSs in the present work to make it fully dependent on measurable quantities (thread spacings, thread diameters, and thickness). The full set of equations consists of seven non-linear equations with eleven parameters (unknowns), from which at least seven must be measured/known to solve the system:

$$c_i = \frac{l_i}{p_i} - 1, \quad (9)$$

$$p_i = (l_i - D\theta_i) \cos \theta_i + D \sin \theta_i \quad (10)$$

$$h_i = (l_i - D\theta_i) \sin \theta_i + D(1 - \cos \theta_i), \quad (11)$$

$$D = h_x + h_y, \quad (12)$$

$$h_x = (D_{hx} + D_{hy}) \left(1 - \frac{1}{\cos \theta_x}\right) + (L_{px} + D_{hy}) \tan \theta_x, \quad (13)$$

where  $p_i$  is the spacing between centres of threads ( $p_i = L_{pi} + D_{hi}$ ),  $c_i$  is the fractional crimp,  $l_i$  is the total length of the thread,  $\theta_i$  are the contact angles/inclination of the central straight part of the threads,  $p_i$  is the horizontal spacing of threads,  $\theta_i$  is the angle with respect to the horizontal plane, and  $h_i$  is the vertical displacement of the threads. The subscript  $i = x, y$  is used to differentiate the warp and weft threads by their coordinates (see Figure 2). All the dimensions are relatable by trigonometric relations, not shown in this work for the sake of simplicity, but we suggest the reader to see [17] for further details.

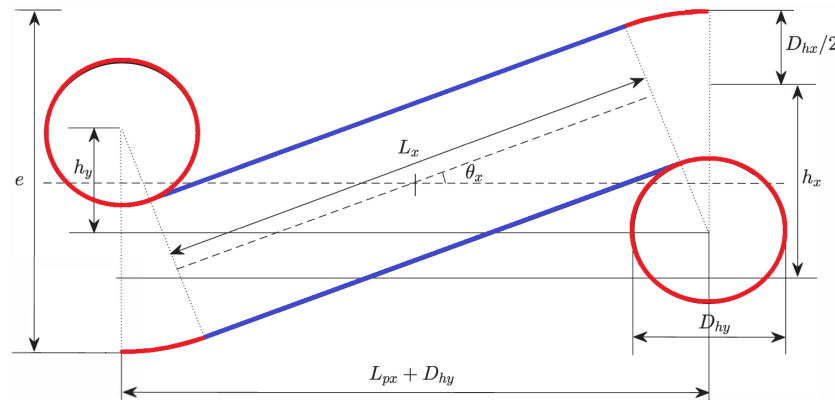


**Figure 2.** Example of application of the non-linear model to the x-thread of a IPS. For an y-thread, x-related parameters must be swapped by y-related parameters and vice versa. Straight cylindrical part of inclination  $\theta_x$  represented in blue color.

By solving the non-linear set of Equations (9)–(13), Equation (8) can be further developed. The calculation of the volumetric porosity can be then finally written as:

$$\phi_{3D} = 1 - \pi \frac{D_{hx}L_x + D_{hx}^2(D_{hx} + D_{hy})\theta_x + D_{hy}L_y + D_{hy}^2(D_{hx} + D_{hy})\theta_y}{4e(L_{px} + D_{hy})(L_{py} + D_{hx})}, \quad (14)$$

where  $e$ ,  $L_{px}$ ,  $L_{py}$ ,  $D_{hx}$  and  $D_{hy}$  are measurements, and  $\theta_x$ ,  $\theta_y$ ,  $L_x$  and  $L_y$  are obtained from the calculations. Equation (14) represents a function to connect all the required geometric parameters to know the volumetric porosity analytically. Although there are few softwares out there to obtain certain geometric characteristics of the screens and their two-dimensional porosity [14], the only software in the literature to obtain the three-dimensional porosity is Poro3D v1.0 [16]. From certain geometric inputs, this software estimates the volumetric porosity of screens, as well as the 3D representation of the interlaced threads, as shown in Figure 1.

### 3. Modelling Results

A total of 31 IPSs have been used in this work. Different steps were necessary to develop the models. First, the two-dimensional geometric characteristics have been obtained by using the Euclides software [14]. Second, in order to calculate the three-dimensional porosity, it is necessary to know the thickness of the IPSs. The thickness was measured with non-contact measuring equipment (non-contact optical measurement) [1]. Third, the 31 IPSs were tested experimentally in a low-speed wind tunnel, by obtaining the values

of the parameters  $a$  and  $b$  from Equation (1), and determining the values of  $K_p$  and  $Y$  for each IPS, by following the approach explained in Lopez et al. [1]. Tables 1 and 2 present the geometric and aerodynamic characterization of the 31 IPS, respectively. Pressure drop caused by the presence of the insect-proof screens has been measured experimentally in a wind tunnel designed&manufactured at the University of Almeria [1,20,32]. The wind tunnel is 4.74 m long, with a diameter test section of 0.388 m. For each IPS, three tests were carried out with three random samples. To measure the pressure drop, two Pitot pipes (Airflow Developments Ltd; 4 mm of diameter) and a differential pressure transducer SI727 (Special Instruments; operational range of 0–200 Pa and accuracy of  $\pm 0.25\%$ ) were used. To measure the velocity and temperature of air, a hot-wire anemometer EE70-VT32C5 (Elektronik Engerwitzdorf, measurement range of 0–10 m s<sup>-1</sup> and 0–50 °C; accuracy of  $\pm 0.2$  m s<sup>-1</sup> + 2% of measuring value and  $\pm 0.2$  °C) was used. For further information on the wind tunnel characteristics, please see [21].

**Table 1.** Geometric and porosity data of IPSs. The parameters are: IPS number ( $N_{IPS}$ ), density of threads ( $\rho_t$ , in threads/cm<sup>2</sup>), 2D porosity ( $\phi_{2D}$ , [m<sup>2</sup> m<sup>-2</sup>]), 3D porosity ( $\phi_{3D}$ , [m<sup>3</sup> m<sup>-3</sup>]),  $x$  and  $y$  lengths of the pore ( $L_{px}$  and  $L_{py}$ , [ $\mu$ m]), diameters of the weft and warp threads ( $D_{hx}$  and  $D_{hy}$ , respectively, [ $\mu$ m]), average diameter of threads ( $D_h$ , [ $\mu$ m]), diameter of the inside circumference of the pore ( $D_i$ , [ $\mu$ m]), and thickness ( $e$ , [m]).

$N_{IPS}$	$\rho_t$	$\phi_{2D}$	$\phi_{3D}$	$L_{px}$	$L_{py}$	$D_{hx}$	$D_{hy}$	$D_h$	$D_i$	$e \times 10^{-6}$
1	11 × 23	0.322	0.704	197.0	709.5	248.2	254.4	251.3	202.0	589
2	10 × 20	0.369	0.734	243.7	774.0	251.6	253.5	252.5	248.5	596
3	10 × 20	0.366	0.715	232.5	760.7	233.1	253.1	243.1	237.4	544
4	10 × 20	0.349	0.709	226.9	681.1	256.8	243.5	250.2	232.1	567
5	10 × 20	0.402	0.730	252.9	806.9	223.4	238.5	230.9	257.5	501
6	10 × 20	0.310	0.666	199.2	710.8	264.4	267.1	265.7	203.7	571
7	10 × 20	0.402	0.752	246.8	877.3	233.8	236.5	235.1	249.8	546
8	14 × 27	0.379	0.723	187.3	543.5	186.5	184.0	185.2	192.5	418
9	10 × 20	0.378	0.735	253.9	784.3	250.5	253.5	252.0	255.8	587
10	10 × 20	0.375	0.733	251.7	863.6	264.4	260.7	262.5	256.0	604
11	10 × 20	0.375	0.736	250.3	865.1	264.6	260.3	262.4	255.8	611
12	10 × 20	0.368	0.7453	252.7	746.4	259.0	255.7	257.3	255.2	639
13	14 × 27	0.292	0.6876	141.8	615.9	214.8	221.7	218.3	144.2	514
14	14 × 27	0.267	0.6548	131.8	570.5	209.6	225.7	217.7	134.1	490
15	10 × 20	0.338	0.6859	207.4	756.6	253.4	251.8	252.6	210.7	540
16	15 × 30	0.556	0.8302	221.6	548.8	110.5	109.9	110.1	222.9	261
17	18 × 31	0.520	0.8093	209.0	427.7	110.6	110.2	110.4	210.3	259
18	16 × 30	0.368	0.7125	162.2	458.4	163.1	162.8	162.9	164.0	362
19	14 × 30	0.385	0.7364	162.6	540.6	159.8	163.5	161.9	165.0	371
20	12 × 30	0.405	0.7612	166.7	663.6	164.7	162.9	163.6	169.6	388
21	10 × 30	0.437	0.7951	170.9	876.8	163.3	160.0	161.2	174.5	406
22	10 × 30	0.446	0.8090	173.0	900.9	158.1	158.4	158.3	177.2	419
23	13 × 30	0.390	0.7509	164.6	593.3	168.6	163.1	165.5	167.4	392
24	10 × 20	0.335	0.6643	233.7	734.0	276.4	273.4	274.5	236.6	564
25	14 × 27	0.385	0.7207	188.4	591.6	184.1	184.7	184.4	191.3	402
26	10 × 20	0.375	0.7107	234.9	838.7	245.8	248.0	247.2	238.7	526
27	13 × 30	0.263	0.6673	110.0	611.9	187.7	209.4	200.2	113.5	458
28	10 × 20	0.350	0.6877	238.6	746.0	272.0	261.2	265.3	241.7	564
29	15 × 30	0.237	0.6626	107.5	456.3	196.0	211.1	204.7	110.7	508
30	10 × 20	0.381	0.7130	254.1	777.7	253.6	247.2	249.6	257.2	535
31	10 × 20	0.354	0.6774	240.0	761.5	264.0	261.8	262.6	242.8	535

**Table 2.** Aerodynamic data of the IPSs. The parameters are: IPS number ( $N_{IPS}$ ), pressure drop coefficients ( $a$  and  $b$ ), goodness of fit of the pressure drop model with the estimated  $a$  and  $b$  coefficients ( $R^2$ ), and permeability ( $K_p$ , [m<sup>2</sup>]) and inertial factor ( $Y$ ) from experimental measurements with the pressure drop model (actual value).

$N_{IPS}$	$a$	$b$	$R^2$	$K_p$	$Y$
1	2.784	3.045	0.9997	$3.512 \times 10^{-9}$	0.233
2	2.102	2.676	0.9928	$4.041 \times 10^{-9}$	0.187
3	2.036	2.253	0.9983	$4.386 \times 10^{-9}$	0.206
4	2.407	2.876	0.9988	$3.576 \times 10^{-9}$	0.212
5	1.767	1.676	0.9993	$5.432 \times 10^{-9}$	0.216
6	3.029	3.792	0.9976	$2.731 \times 10^{-9}$	0.231
7	1.519	1.534	0.9997	$6.461 \times 10^{-9}$	0.186
8	1.879	3.074	0.9990	$2.467 \times 10^{-9}$	0.186
9	1.909	2.375	0.9987	$4.484 \times 10^{-9}$	0.181
10	1.845	1.876	0.9995	$5.849 \times 10^{-9}$	0.194
11	1.852	1.899	0.9990	$5.835 \times 10^{-9}$	0.193
12	1.947	2.176	0.9986	$5.331 \times 10^{-9}$	0.185
13	3.182	5.440	0.9992	$1.716 \times 10^{-9}$	0.213
14	3.595	6.006	0.9997	$1.480 \times 10^{-9}$	0.235
15	2.284	3.051	0.9994	$3.211 \times 10^{-9}$	0.200
16	0.870	2.635	0.9993	$1.793 \times 10^{-9}$	0.118
17	0.824	2.744	0.9992	$1.713 \times 10^{-9}$	0.110
18	2.235	4.738	0.9996	$1.386 \times 10^{-9}$	0.192
19	1.896	3.749	0.9997	$1.798 \times 10^{-9}$	0.180
20	1.575	3.179	0.9992	$2.216 \times 10^{-9}$	0.159
21	1.302	2.683	0.9993	$2.745 \times 10^{-9}$	0.140
22	1.261	2.645	0.9949	$2.876 \times 10^{-9}$	0.134
23	1.669	3.885	0.9995	$1.853 \times 10^{-9}$	0.155
24	2.562	4.159	0.9992	$2.453 \times 10^{-9}$	0.187
25	2.038	3.585	0.9994	$2.028 \times 10^{-9}$	0.190
26	1.913	1.844	0.9968	$5.183 \times 10^{-9}$	0.218
27	3.886	5.802	0.9992	$1.439 \times 10^{-9}$	0.269
28	2.452	3.262	0.9992	$3.154 \times 10^{-9}$	0.204
29	5.872	6.111	0.9995	$1.514 \times 10^{-9}$	0.377
30	2.089	1.506	0.999	$6.427 \times 10^{-9}$	0.260
31	2.163	2.861	0.998	$3.417 \times 10^{-9}$	0.199

As outlined before, the main purpose of the present investigation is to improve the classical modelling based on two-dimensional data only by adding a three-dimensional estimation of porosity. In Figure 3, the 2D and 3D characteristics of the 31 IPSs are explored by the projected pore area vs exact 3D area of screens according to [33] (Figure 3a) and the 2D vs. 3D porosities (Figure 3b). In these Figures, it can be seen that the variation of two-dimensional parameters is different from the variation of three-dimensional parameters amongst the same screens. There may be scenarios in which two screens with equal two-dimensional geometric parameters, when compared to three-dimensional geometric parameters, are actually different. For instance, two IPSs that have the same two-dimensional porosity but different thicknesses may have a different effect on the airflow through them, since they present different three-dimensional porosity characteristics [17]. Thus, the conclusion is that the real porosity (three-dimensional) is not the same between these two IPSs, and thus the performance cannot be the same, as always considered in previous literature.

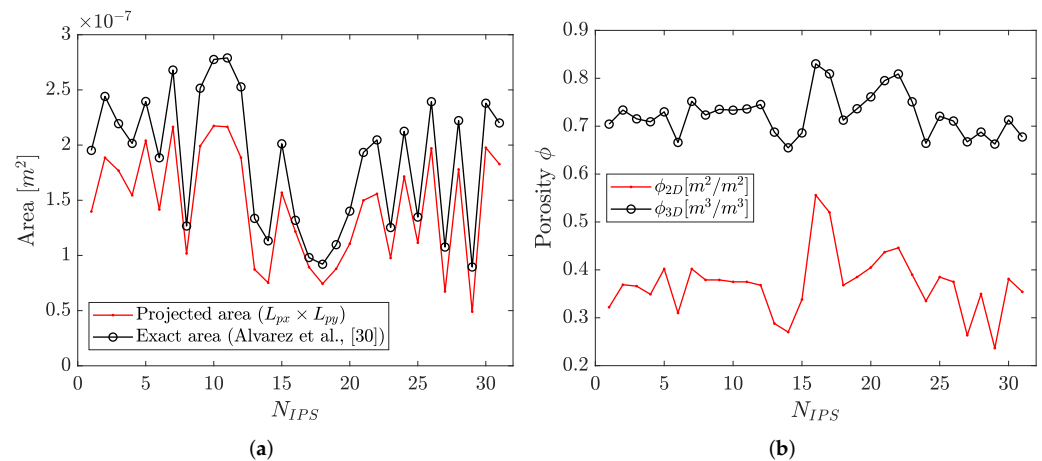


**Figure 3.** Comparison between (a) orthogonal projection and exact 3D effective pore areas, and (b) two and three-dimensional (volumetric) porosities according to [17].

### 3.1. 3D-Based Permeability Model for Insect-Proof Screens

Permeability is one of the most influential aspects in the estimation of the aerodynamic performance of screens, as denoted in the Forchheimer equation (Equation (2)). In Lopez et al. [1] a new model for the permeability of insect-proof screens was proposed, which had a very acceptable performance. This model has the form in Equation (4), where  $D_h$  stands for the average diameter of the threads and  $\phi_{2D}$  stands for the two-dimensional porosity. The model demonstrated to be a much more accurate option than the models provided in [18] (dependent solely on two-dimensional porosity  $\phi_{2D}$ ). However, the models proposed in Lopez et al. [1], still have room for improvement. In their work, the modelling was focused on experimental  $K_p$  data directly by improving the empirical  $K_p$  equation previously suggested by Kozeny (Equation (3)). Although this is a good approach, they omitted an interesting and relevant point: since the observed (experimental) values of  $K_p$  are originally obtained from using experimental pressure drop data and substitution in the Forchheimer equation (see Equation (2)), it is smarter to find a way to estimate the Forchheimer equation coefficients directly. Moreover, a volumetric estimation of porosity would be more accurate than a superficial one. Thus, in the present work, an improvement on the permeability model is suggested, in terms of estimation (directly modelling the Forchheimer equation coefficients) and modelling porosity as a three-dimensional property.

The suggested  $K_p$  model is of the form  $K_p = K_p(e, D_i, \mu, \phi)$ , either denoted as  $K_{p,2D}$  or  $K_{p,3D}$  depending on the chosen porosity  $\phi$ :

$$K_p = \frac{e\mu}{b} = \frac{e\mu}{\alpha_1 + \alpha_2 D_i + \alpha_3 \phi'} \tag{15}$$

where a linear fit with coefficients  $\alpha_i$  was tested successfully for  $b$ . The only coefficient involved in the  $K_p$  equation is  $b$ , and to model this coefficient is a much better option than modelling  $K_p$  observed values as in the previous literature because we have observed a very strong linearity in this estimated coefficient in  $\Delta P$  fits (see Figure 4). This is an important improvement, because to model a linear behaviour is always less prone to errors and usually much more generalisable. This  $K_p$  model was tested for  $\phi$  being either a two-dimensional ( $\phi_{2D}$ ) or three-dimensional porosity ( $\phi_{3D}$ ). Similarly to the model in Equation (4), the two-dimensional approach to porosity provided a model  $K_{p,2D}$  that failed at predicting  $K_p$  for the two values of highest superficial porosity ( $N_{IPS} = 16$  and  $17$ ), see outliers in Figure 5. However, the use of the three-dimensional porosity led to a very promising model  $K_{p,3D}$  for permeability. This model outperforms by far the one given in Lopez et al. [1], which had a  $R^2 = 0.56$ . The new model yields an outstanding  $R^2 = 0.81$ , with the fitting constants:  $[\alpha_1, \alpha_2, \alpha_3] = [13.6386, -20, 437.072, -8.6898]$ . The coefficients are estimated by means of a non-linear least squares algorithm [34] with a tolerance of  $10^{-20}$  and a

maximum of  $1 \times 10^5$  iterations, to ensure a converged solution to the inverse problem. The mean relative errors in the prediction ( $\epsilon = \frac{E(|predicted - actual|)}{actual} \times 100$ ) were  $\epsilon_{K_{p,2D}} = 71.557\%$  and  $\epsilon_{K_{p,3D}} = 14.343\%$ , respectively. Must be outlined that despite other more mainstream methods such as deep learning neural networks or similar could be deployed and possibly better predictions could be found, this is not a recommended practice when looking for models in engineering, since these deep learning models are like black-boxes [35] and nobody knows how to interpret the underlying relations between variables because of the impenetrability [36,37]. Actually, in certain fields of finance, these models are forbidden by regulators because they are not interpretable [38]. Researchers are spending great efforts into making it more interpretable [39], but this is still (and perhaps will always be) an issue. Our proposed parametric equations are low degree polynomials, which also guarantee no overfitting, another potential inconvenient in other mentioned methods.

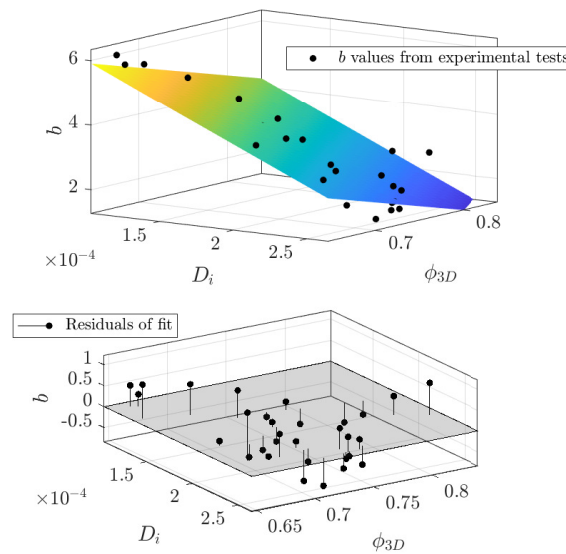


Figure 4. Fitness of  $b$  coefficient using experimental data.

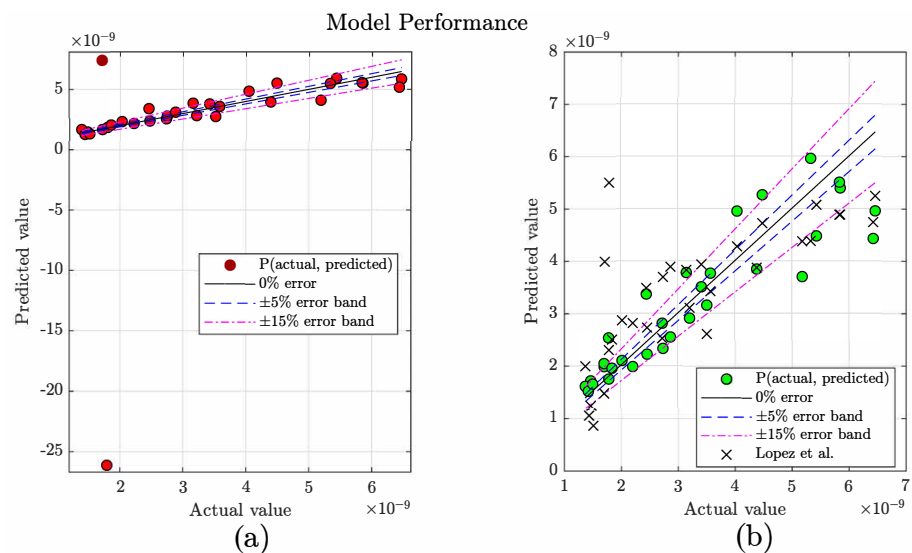


Figure 5. Predictive accuracy for  $K_p$  models. (a) Predictions of Equation (15) with  $\phi_{2D}$  ( $K_{p,2D}$ ). (b) Predictions of Equation (15) with  $\phi_{3D}$  ( $K_{p,3D}$ ) and comparison with the model suggested in Lopez et al. [1].

Therefore, the new proposed model for  $K_p$  can be written as:

$$K_p = \frac{e\mu}{13.6386 - 20437.072D_i - 8.6898\phi_{3D}}. \quad (16)$$

This model is simpler than previous works in the literature (see, for instance [1,18,23]), and surpassed the predictive performance of the best model to date, the one proposed in Lopez et al. [1]. From Figure 5 can be seen the performance of the  $K_p$  model with two-dimensional (Figure 5a) and three-dimensional porosity (Figure 5b). To use two-dimensional porosity has been found very unacceptable in our proposed model, as Figure 5a shows two screens very far from the trend ( $N_{IPS} = 16$  and 17, the ones with highest porosity), one of them even yielding a non-positive value for permeability. But even more surprisingly, also in the model proposed by Lopez et al. [1], those screens are also appearing as outliers in Figure 5b. However, when the three-dimensional porosity is used in the development of our proposed model, most screens lay within a  $\pm 15\%$  error band. Thus, it is evident that the use of  $\phi_{2D}$  in the models is wrong and leads to misleading models. Next, to fully describe the aerodynamics of IPSs, the inertial factor  $Y$  must be also modelled including the three-dimensional porosity as parameter.

### 3.2. 3D-Based Inertial Factor Model for Insect-Proof Screens

The modelling scenario for the other parameter necessary to characterise the aerodynamics of these screens, the inertial factor  $Y$ , has been frequently considered independent from  $K_p$  in the literature. For instance, in [1] a new model for  $Y$  was validated (Equation (4)). Similar models are actually found in other works from the literature such as Betchen et al. [40], where a model  $Y = A_1 \times \phi^{-|A_2|}$  is suggested, where  $A_1$  and  $A_2$  stand for the coefficients of the model. The model in Equation (6) suggested in Lopez et al. [1] provided superior performance to the models also shown in Miguel [18]. However, as observed e.g., in the review on non-Darcy coefficients (equivalent to inertial coefficients) shown in Li & Engler [41], some scientists observed that  $Y$  has strong relation with  $K_p$  and  $\phi$  and included this term in their empirical correlations for  $Y$ . Thus, the correlation model given in Equation (6) from Lopez et al. [1] can be improved by including more influential parameters in the modelling. In [1] is also suggested from fitting the Forchheimer equation with experimental data that  $Y$  can be written as:

$$Y = \frac{a\sqrt{K_p}}{e\rho}, \quad (17)$$

where  $a$  is the fitting constant in the term of  $u^2$  of the Forchheimer equation and  $\rho$  is the fluid density. By using the model found in Equation (15), the equation can be rewritten as:

$$Y = \frac{a\sqrt{\frac{e\mu}{\alpha_1 + \alpha_2 D_i + \alpha_3 \phi_{3D}}}}{e\rho}. \quad (18)$$

Thus the expression can be only dependent on porosity and geometry if the  $a$  coefficient is modelled suitably. For this aim, the coefficient has been modelled by means of relations of  $\phi_{3D}$ , and the diameter ratio  $D_h/D_i$  as in Equation (6). After testing several combinations, the best equation to model  $a$  has been selected as a second degree polynomial for  $D_h/D_i$  and first degree for  $\phi_{3D}$ , plus a nonlinear interaction between both variables:

$$a = \beta_{00} + \beta_{10} \frac{D_h}{D_i} + \beta_{01} \phi + \beta_{20} \left( \frac{D_h}{D_i} \right)^2 + \beta_{11} \left( \frac{D_h}{D_i} \right) \phi_{3D}, \quad (19)$$

where  $\beta_{ij}$  are the fitting coefficients. The coefficients are estimated by means of a Levenberg-Marquardt nonlinear least squares algorithm [34,42] with a tolerance of 1E-6 and a max-

imum of 400 iterations and 600 function evaluations. The fitness function is shown in Figure 6, whose fitting coefficients are:

$$[\beta_{00}, \beta_{10}, \beta_{01}, \beta_{20}, \beta_{11}] = [10.434, -5.420, -11.922, 1.159, 6.137]. \quad (20)$$

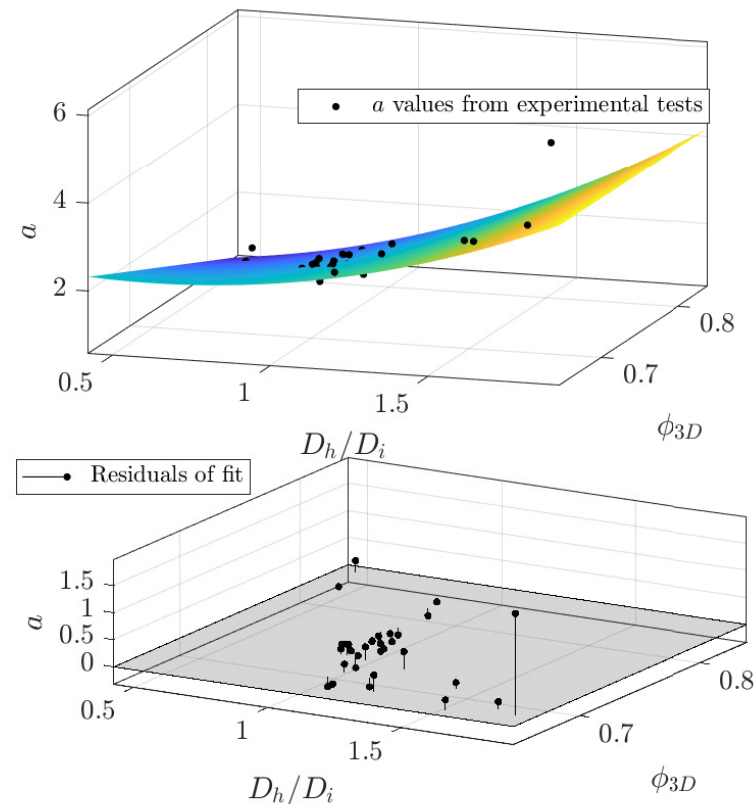


**Figure 6.** Fitness of  $a$  coefficient from experimental data.

Must be outlined that, since the proposed model actually depends on  $K_p$ , the prior modelling errors are propagated to the new prediction, being difficult to improve the model for  $Y$  from this base. Actually, the  $R^2$  goodness of fit for the  $a$  coefficient according to Equation (19) and shown in Figure 6 reaches a  $R^2 \approx 0.92$ . The goodness of fit could even reach a  $R^2 \approx 0.94$  if the highest residual in Figure 6 is deleted, but it is kept in the analysis for consistency reasons. The model found for  $Y$  has a mean relative error in the prediction of  $\epsilon_Y = 6.668\%$  only and the performance is shown in Figure 7 against predictions by the  $Y$  model published in Lopez et al. [1].

In Figure 7 can be seen that the performance of our proposed model is outstanding, with most data within the  $\pm 5\%$  error band, whilst most predictions of Lopez et al. [1] lay outside the  $\pm 15\%$  error band. Thus, the new equation for  $Y$  enables a relationship  $Y = Y(e, \rho, \mu, D_h, D_i, \phi_{3D})$ , from a **two-step modelling** ( $K_p$  was previously modelled) which clearly outperforms the model given in Equation (6) from Lopez et al. [1]. An important improvement we did with respect to the model given in Lopez et al. [1] (as well as those provided in Nield & Bejan [23], Miguel [18], Beavers et al. [27], and Ergun [43]), is that our proposed model is dependent on porosity, which is a parameter of strong influence in the inertial factor, whilst the equation provided in Lopez et al. only depends on  $D_h$  and  $D_i$  (Equation (6)). Therefore, generally speaking, since it is very intuitive that the inertial factor has strong dependence on the said parameters (thickness of the screen, density, viscosity, average diameter of threads, inner circumference diameter of the pore, and porosity), we can undoubtedly say that our new proposed model for  $Y$  is more descriptive of the actual values and provides a more complete explanation of this parameter by adapting more to reality.

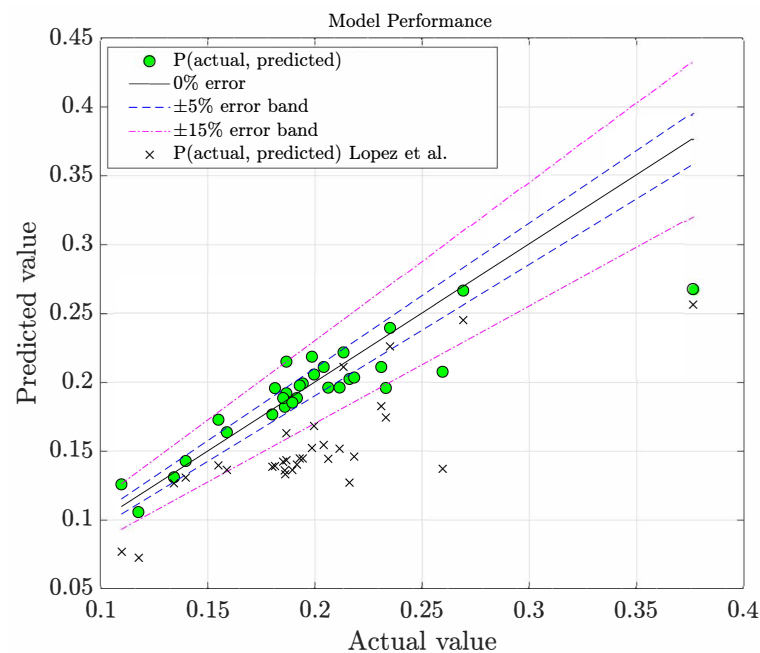


**Figure 7.** Predictive accuracy for  $Y$  models. Predictions of Equation (18) with three-dimensional porosity. Performance compared to Equation (6) predictions from Lopez et al. [1].

#### 4. Discussion

The present work has been focused on the improvement of models for the two most influential parameters in the modelling of pressure drop of flow-past-screens: permeability and inertial factor. Pressure drop can be modelled as a second degree polynomial, as shown in Equation (2), thus a nested-like model approach has been intended to model the pressure drop coefficients aiming to find good models to estimate permeability and inertial factor.

To model permeability, it has been observed that the diameter of the inner circumference of the pore  $D_i$  is a very good candidate for the model, as done in [1]. Other pore and thread related parameters such as the average diameter of threads  $D_h$ , the  $D_{hx}/D_{hy}$  thread ratio, or the  $D_h/D_i$  ratio have been tried as model parameter, but these performed considerably worse than  $D_i$ . It was also very relevant the improvement found when a three-dimensional porosity was used as model parameter instead of the two-dimensional one. Specially because there are some IPSs performances which are difficult to be predicted, possibly because the duality found in the thickness: two screens may have the same 2D porosity, but different thickness, which leads to different pressure drop. Therefore, a model dependent on two-dimensional quantities may struggle to predict the performance of certain screens.

For the inertial factor, it has been investigated that to add porosity as model parameter is of strong importance. This is in contrast to other previous works, which modelled this parameter with simpler parameter relations, and did not include porosity nor permeability as relevant features (see, for instance, Equations (5) and (6)). It was obvious to us that permeability must be included, since  $Y$  is actually defined upon this parameter in the Forchheimer model in Equation (2). In addition, it was also clear to us that porosity should be included in the model of  $Y$ , and the outstanding modelling results obtained from this investigation confirmed this guess. To model the inertial factor, it is necessary to use the permeability model and a model for the  $a$  coefficient. Despite of the expected propagation of modelling errors, it is very surprising that this new model outperforms by far the best model to date from the literature, as seen in Figure 7.

To sum up, the new models for  $K_p$  and  $Y$  based on the three-dimensional porosity of screens provide an important contribution to the characterisation of screens, as they allow to estimate the aerodynamic performance of IPSs with high accuracy. Both models are based on relevant parameters, and are fully parametric with no black-box predictions as

deep learning algorithms do, being often the performance quite obscure as it is not possible to interpret what happens inside the decision algorithms.

## 5. Conclusions

This investigation has been focused on the development of novel models for permeability  $K_p$  and inertial factor  $Y$ , for the characterisation of the performance of insect-proof screens (IPSs) as a three-dimensional porous medium. Instead of fitting models directly on observable training data values of  $K_p$  and  $Y$  (as done by all previous authors in the literature), a smarter approach was carried out, which was based on focusing the modelling efforts on finding models for the constants in the pressure drop of Forchheimer equation. This modelling approach includes the three-dimensional porosity as modelling parameter for the first time, since the software Poro3D [16,17] allows to obtain this parameter analytically for any screen.

The combination of all these aspects has led to models that obtain much better predictions than the existing ones by Lopez et al. [1] in the literature, which are the best to date. In the performance of the proposed models for  $K_p$ , it has been observed that the new models have most data within a  $\pm 15\%$  error band (the relative error of this proposed model is a 14.34%), whilst the model introduced in Lopez et al. [1] has only few data within this error band. In terms of  $Y$ , the predictive performance of our proposed model is even more outstanding (even though it is a two-step modelled parameter upon the  $K_p$  model), with only two predictions out of 31 laying outside the  $\pm 15\%$  error band, and most data within the  $\pm 5\%$  error band; whilst most predictions of Lopez et al. [1] laid outside the  $\pm 15\%$  error band. Another important aspect in our proposed model for  $Y$  is that this model combines more relevant parameters in the inertial factor dynamics than previous models in the literature, which were too simple (the vast majority of them not even dependent on porosity nor permeability).

The performance of the suggested models is, therefore, an important contribution in the field, since more reliable characterisation of insect-proof screens could be developed. This means that their aerodynamic characteristics can be even predicted before fabrication at design stages. A limitation of the present work is that the size of the training data set could be increased with more different geometries of screens by means of an extensive experimental study. In our opinion, to study experimentally at least 1000 screens could lead to models built upon more geometries and, therefore, one can be more confident with the generalisation of these models. A future study collecting such information could be useful to update the model coefficients of the models suggested in the present work.

**Author Contributions:** Conceptualization, F.-J.G.-O. and A.L.-M.; methodology, F.-J.G.-O.; software, F.-J.G.-O.; validation, F.-J.G.-O. and A.L.-M.; formal analysis, F.-J.G.-O.; investigation, F.-J.G.-O.; resources, A.L.-M., F.D.M.-A., A.P.-F., J.A.M.-L. and D.L.V.-M.; data curation, A.L.-M. and F.D.M.-A.; writing—original draft preparation, F.-J.G.-O.; writing—review and editing, F.-J.G.-O., A.L.-M., F.D.M.-A., C.-H.L., A.P.-F., J.A.M.-L. and D.L.V.-M.; visualization, F.-J.G.-O.; supervision, A.L.-M. and C.-H.L.; project administration, A.L.-M. and D.L.V.-M.; funding acquisition, D.L.V.-M. All authors have read and agreed to the published version of the manuscript.

**Funding:** The first author acknowledges the Ramón y Cajal 2021 Excellence Research Grant action from the Spanish Ministry of Science and Innovation (FSE/AGENCIA ESTATAL DE INVESTIGACIÓN), as well as the Andalusian Research, Development and Innovation Plan (PAIDI—Junta de Andalucía) postdoctorate fundings. Additional support was provided by research project UAL2020-AGR-A1916 within the FEDER-Andalucía 2014–2020 operational program.

**Data Availability Statement:** Data can be provided upon reasonable request.

**Conflicts of Interest:** The authors declare no conflict of interest.

## References

1. López-Martínez, A.; Molina-Aiz, F.; Valera, D.; Espinoza-Ramos, K. Models for characterising the aerodynamics of insect-proof screens from their geometric parameters. *Biosyst. Eng.* **2020**, *192*, 42–55. [CrossRef]
2. Valera, D.; Belmonte, L.; Molina-Aiz, F.; López, A. *Greenhouse Agriculture in Almería. A Comprehensive Techno-Economic Analysis*; Cajamar Caja Rural: Almería, Spain, 2016.
3. Teitel, M. The effect of screened openings on greenhouse microclimate. *Agric. For. Meteorol.* **2007**, *143*, 159–175. [CrossRef]
4. Álvarez, A.J.; Oliva, R.M. Textile Physical Barriers against the Chestnut Gall Wasp *Dryocosmus kuriphilus*. *Agronomy* **2022**, *12*, 1728. [CrossRef]
5. Muñoz, P.; Montero, J.; Antón, A.; Giuffrida, F. Effect of Insect-proof Screens and Roof Openings on Greenhouse Ventilation. *J. Agric. Eng. Res.* **1999**, *73*, 171–178. [CrossRef]
6. Bartzanas, T.; Boulard, T.; Kittas, C. Numerical simulation of the airflow and temperature distribution in a tunnel greenhouse equipped with insect-proof screen in the openings. *Comput. Electron. Agric.* **2002**, *34*, 207–221. [CrossRef]
7. Lopez-Martinez, A.; Martínez, D.L.V.; Molina-Aiz, F.; Peña-Fernandez, A.; Marín-Membrive, P. Microclimate evaluation of a new design of insect-proof screens in a Mediterranean greenhouse. *Span. J. Agric. Res.* **2014**, *12*, 338. [CrossRef]
8. López-Martínez, A.; Granados-Ortiz, F.J.; Molina-Aiz, F.D.; Lai, C.H.; Moreno-Teruel, M.d.l.Á.; Valera-Martínez, D.L. Analysis of Turbulent Air Flow Characteristics Due to the Presence of a 13×30 Threads-cm<sup>2</sup> Insect Proof Screen on the Side Windows of a Mediterranean Greenhouse. *Agronomy* **2022**, *12*, 586. [CrossRef]
9. Kittas, C.; Boulard, T.; Bartzanas, T.; Katsoulas, N.; Mermier, M. Influence Of An Insect Screen On Greenhouse Ventilation. *Trans. ASAE* **2002**, *45*, 1083. [CrossRef]
10. Jatta, E.; Carrasco-Tenezaca, M.; Jawara, M.; Bradley, J.; Ceesay, S.; D'Alessandro, U.; Jeffries, D.; Kandeh, B.; Lee, D.S.H.; Pinder, M.; et al. Impact of increased ventilation on indoor temperature and malaria mosquito density: An experimental study in The Gambia. *J. R. Soc. Interface* **2021**, *18*, 20201030. [CrossRef]
11. Desquesnes, M.; Bouhsira, E.; Chalermwong, P.; Drosne, L.; Duvallat, G.; Franc, M.; Gimonneau, G.; Grimaud, Y.R.P.; Guillet, P.; Himeidan, Y.E.; et al. Insecticide-impregnated screens used under 'multi-target method' for haematophagous fly control in cattle: A proof of concept. In *Ecology and Control of Vector-Borne Diseases*; Wageningen Academic Publishers: Wageningen, The Netherlands, 2021; pp. 201–227.
12. Lv, H.; Chen, X. New insights into the mechanism of fluid mixing in the micromixer based on alternating current electric heating with film heaters. *Int. J. Heat Mass Transf.* **2021**, *181*, 121902. [CrossRef]
13. Lv, H.; Chen, X.; Zeng, X. Optimization of micromixer with Cantor fractal baffle based on simulated annealing algorithm. *Chaos Solitons Fractals* **2021**, *148*, 111048. [CrossRef]
14. Álvarez, A.; Oliva, R.; Valera, D. Software for the geometric characterisation of insect-proof screens. *Comput. Electron. Agric.* **2012**, *82*, 134–144. [CrossRef]
15. López-Martínez, A.; Valera-Martínez, D.; Molina-Aiz, F.; Peña-Fernández, A.; Marín-Membrive, P. Field analysis of the deterioration after some years of use of four insect-proof screens utilized in Mediterranean greenhouses. *Span. J. Agric. Res.* **2013**, *11*, 958–967. [CrossRef]
16. Granados-Ortiz, F.J.; Lopez-Martinez, A.; Arrabal-Campos, F.M. Poro3D v1.0. Available online: <https://rsoftuma.uma.es/en/software/poro3d/> (accessed on 13 December 2021).
17. Granados-Ortiz, F.J.; Manuel, A.C.F.; Lopez-Martinez, A.E.A. On the Estimation of Three-Dimensional Porosity of Insect-Proof Screens. *Comput. Electron. Agric.* **2022**, *193*, 106639. [CrossRef]
18. Miguel, A.F. Airflow through porous screens: From theory to practical considerations. *Energy Build.* **1998**, *28*, 63–69. [CrossRef]
19. Bailey, B.; Montero, J.; Parra, J.; Robertson, A.; Baeza, E.; Kamaruddin, R. Airflow Resistance of Greenhouse Ventilators with and without Insect Screens. *Biosyst. Eng.* **2003**, *86*, 217–229. : 10.1016/S1537-5110(03)00115-6. [CrossRef]
20. Valera, D.; Álvarez, A.; Molina, F. Aerodynamic analysis of several insect-proof screens used in greenhouses. *Span. J. Agric. Res.* **2006**, *4*, 273–279. [CrossRef]
21. Espinoza, K.; Valera, D.L.; Torres, J.A.; López, A.; Molina-Aiz, F.D. An auto-tuning PI control system for an open-circuit low-speed wind tunnel designed for greenhouse technology. *Sensors* **2015**, *15*, 19723–19749. [CrossRef]
22. Molina-Aiz, F.; Valera, D.; Peña, A.; Gil, J.; López, A. A study of natural ventilation in an Almería-type greenhouse with insect screens by means of tri-sonic anemometry. *Biosyst. Eng.* **2009**, *104*, 224–242. [CrossRef]
23. Nield, D.A.; Bejan, A. *Convection in Porous Media*; Springer: New York, NY, USA, 2006; Volume 3.
24. Wieghardt, K. On the resistance of screens. *Aeronaut. Q.* **1953**, *4*, 186–192. [CrossRef]
25. Pinker, R.A.; Herbert, M.V. Pressure loss Associated with Compressible flow through Square-Mesh wire Gauzes. *J. Mech. Eng. Sci.* **1967**, *9*, 11–23. [CrossRef]
26. Linker, R.; Tarnopolsky, M.; Seginer, I. Increased resistance to flow and temperature-rise resulting from dust accumulation on greenhouse insect-proof screens. In Proceedings of the 2002 ASAE Annual Meeting. American Society of Agricultural and Biological Engineers, Chicago, IL, USA, 28–31 July 2002; p. 1.
27. Beavers, G.; Sparrow, E.M.; Rodenz, D. Influence of bed size on the flow characteristics and porosity of randomly packed beds of spheres. *J. Appl. Mech.* **1973**, *40*, 655–660. [CrossRef]

28. Nie, L.; Yin, Y.; Yan, L.; Zhou, S. Pressure Drop Measurements and Simulations for the Protective Mesh Screen Before the Gas Turbine Compressor. In Proceedings of the 2nd International Conference on Green Energy, Environment and Sustainable Development (GEESD2021), Shanghai, China, 26–27 June 2021; IOS Press: Beijing, China, 2021; pp. 206–216.
29. Oshinowo, L.; Kuhn, D.C. Turbulence decay behind expanded metal screens. *Can. J. Chem. Eng.* **2000**, *78*, 1032–1039. [[CrossRef](#)]
30. Peirce, F.T. 5—The geometry of cloth structure. *J. Text. Inst. Trans.* **1937**, *28*, T45–T96. [[CrossRef](#)]
31. Martínez, A.L.; Aiz, F.D.M.; Martínez, D.L.V.; Fernández, A.A.P.; Espinoza, K. Effect of material ageing and dirt on the behaviour of greenhouse insect-proof screens. *Span. J. Agric. Res.* **2018**, *16*, 4.
32. Molina-Aiz, F.; Valera, D.; Alvarez, A.; Madueño, A. A wind tunnel study of airflow through horticultural crops: Determination of the drag coefficient. *Biosyst. Eng.* **2006**, *93*, 447–457. [[CrossRef](#)]
33. Álvarez, A.; Oliva, R.; Jiménez-Vargas, A.; Villegas-Vallecillos, M. A three-dimensional approach to the porous surface of screens. *J. Text. Inst.* **2019**, *110*, 639–646. [[CrossRef](#)]
34. Seber, G.A.; Wild, C.J. *Nonlinear Regression*; John Wiley & Son: Hoboken, NJ, USA, 2003.
35. Borgelt, C.; Höppner, F.; Klawonn, F. *Guide to Intelligent Data Analysis*; Springer: New York, NY, USA, 2010.
36. Breiman, L. Random forests. *Mach. Learn.* **2001**, *45*, 5–32. [[CrossRef](#)]
37. Granados-Ortiz, F.J.; Ortega-Casanova, J. Machine Learning-Aided Design Optimisation of a Mechanical Micromixer. *Phys. Fluids* **2021**, *33*, 063604. [[CrossRef](#)]
38. Chen, D.; Ye, W.; Ye, J. Interpretable Selective Learning in Credit Risk. *arXiv* **2022**, arXiv:2209.10127.
39. Li, X.; Xiong, H.; Li, X.; Wu, X.; Zhang, X.; Liu, J.; Bian, J.; Dou, D. Interpretable deep learning: Interpretation, interpretability, trustworthiness, and beyond. *Knowl. Inf. Syst.* **2022**, *64*, 3197–3234. [[CrossRef](#)]
40. Betchen, L.; Straatman, A.G.; Thompson, B.E. A nonequilibrium finite-volume model for conjugate fluid/porous/solid domains. *Numer. Heat Transf. Part Appl.* **2006**, *49*, 543–565. [[CrossRef](#)]
41. Li, D.; Engler, T.W. Literature review on correlations of the non-Darcy coefficient. In Proceedings of the SPE Permian Basin Oil and Gas Recovery Conference, Midland, TX, USA, 15–16 May 2001.
42. Moré, J.J. The Levenberg-Marquardt algorithm: Implementation and theory. In *Numerical Analysis*; Springer: New York, NY, USA, 1978; pp. 105–116.
43. Ergun, S. Fluid flow through packed columns. *Chem. Eng. Prog.* **1952**, *48*, 89–94.

**Disclaimer/Publisher’s Note:** The statements, opinions and data contained in all publications are solely those of the individual author(s) and contributor(s) and not of MDPI and/or the editor(s). MDPI and/or the editor(s) disclaim responsibility for any injury to people or property resulting from any ideas, methods, instructions or products referred to in the content.